Appendix A: Additional figures

In the main body of the paper, we showed maps and plots for the Chamaeleon-Musca and Ophiuchus fields. In this appendix we show similar figures for the remaining eight fields, in the same order as in Tables 1 and 2. We first show maps similar to Fig. 3 (Figs. A.1 to A.8), then distribution functions of p and $N_{\rm H}$ similar to Fig. 4 (Figs. A.9 to A.16), and finally distribution functions of $\mathcal{S}(\delta = 16')$ and p similar to Fig. 7 (Figs. A.17 to A.24).

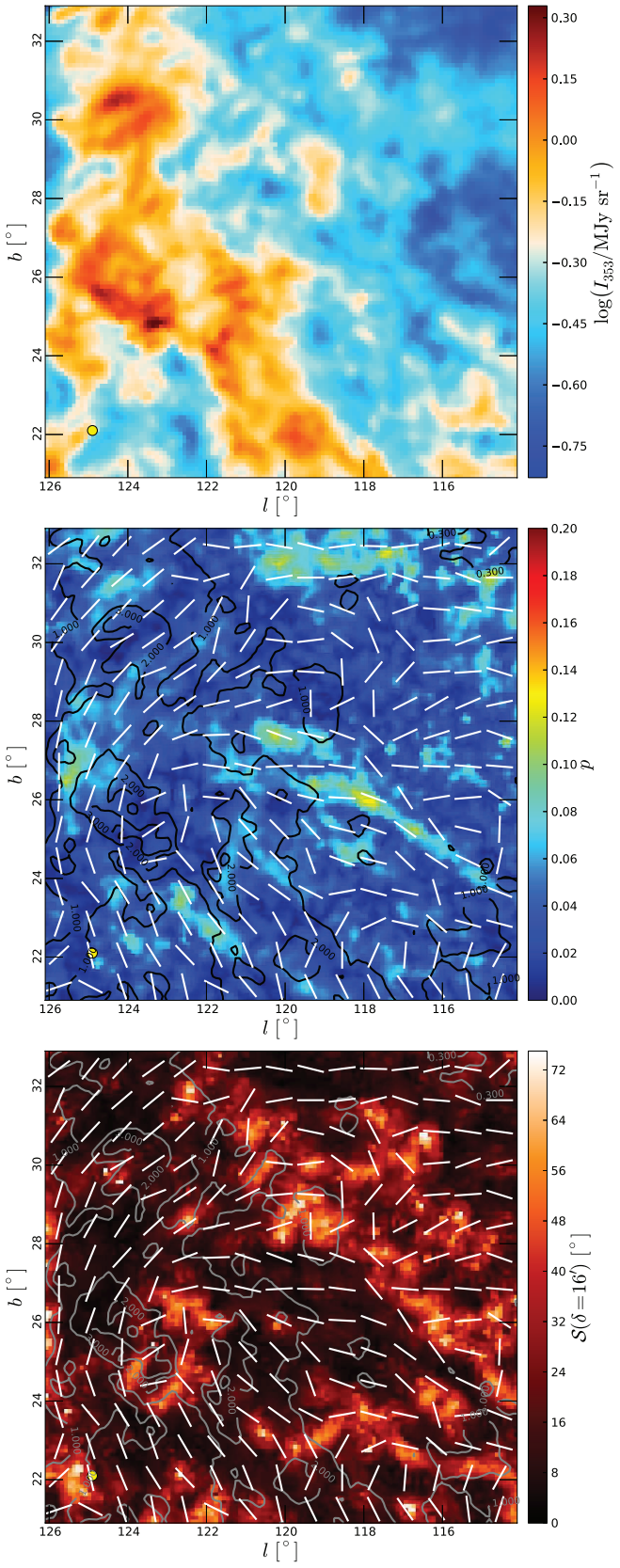

Fig. A.1. Same as Fig. 3, but for the Polaris Flare field. *Top*: total intensity at 353 GHz. *Middle*: polarization fraction p, column density $N_{\rm H}$ (contours in units of 10^{21} cm^{-2}), and magnetic orientation (bars). *Bottom*: angle dispersion function $\mathcal{S}$ with lag $\delta = 16'$ (see Sect. 2.5) with contours and bars identical to the middle row. Note that contours levels are different from those of Fig. 3.

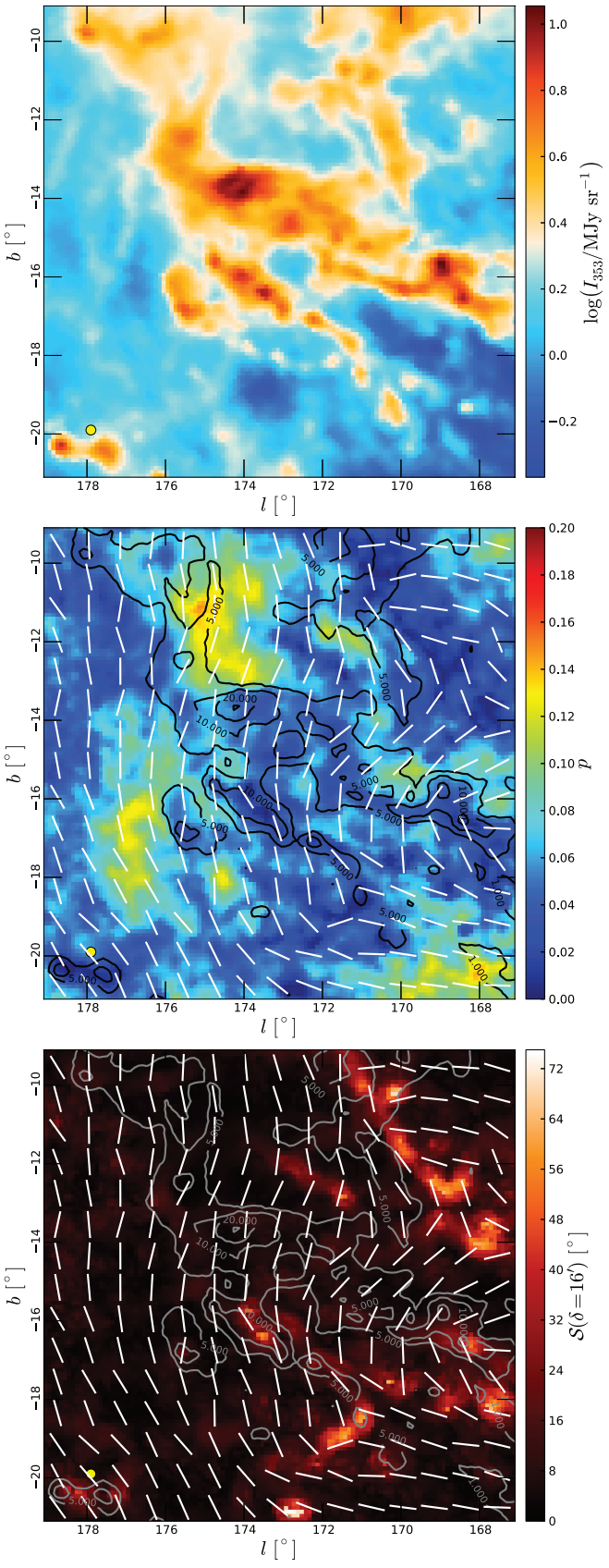

Fig. A.2. Same as Fig. 3, but for the Taurus field.

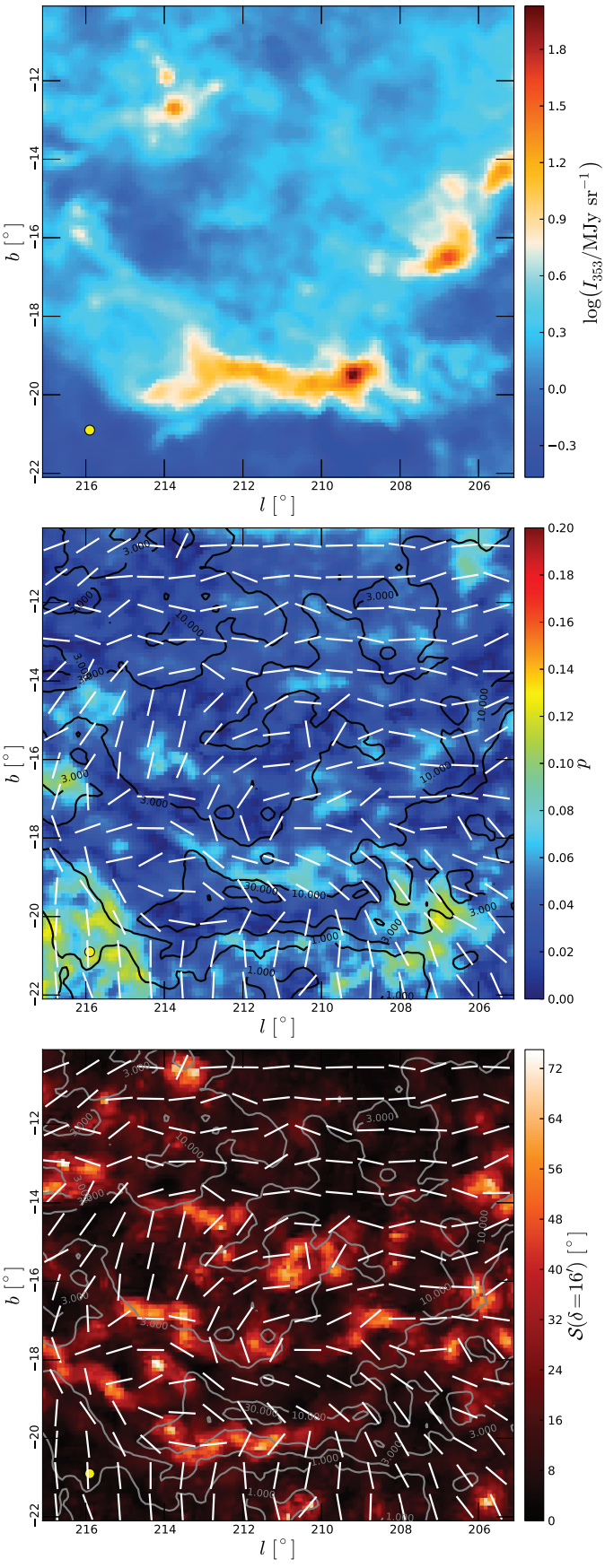

Fig. A.3. Same as Fig. 3, but for the Orion field.

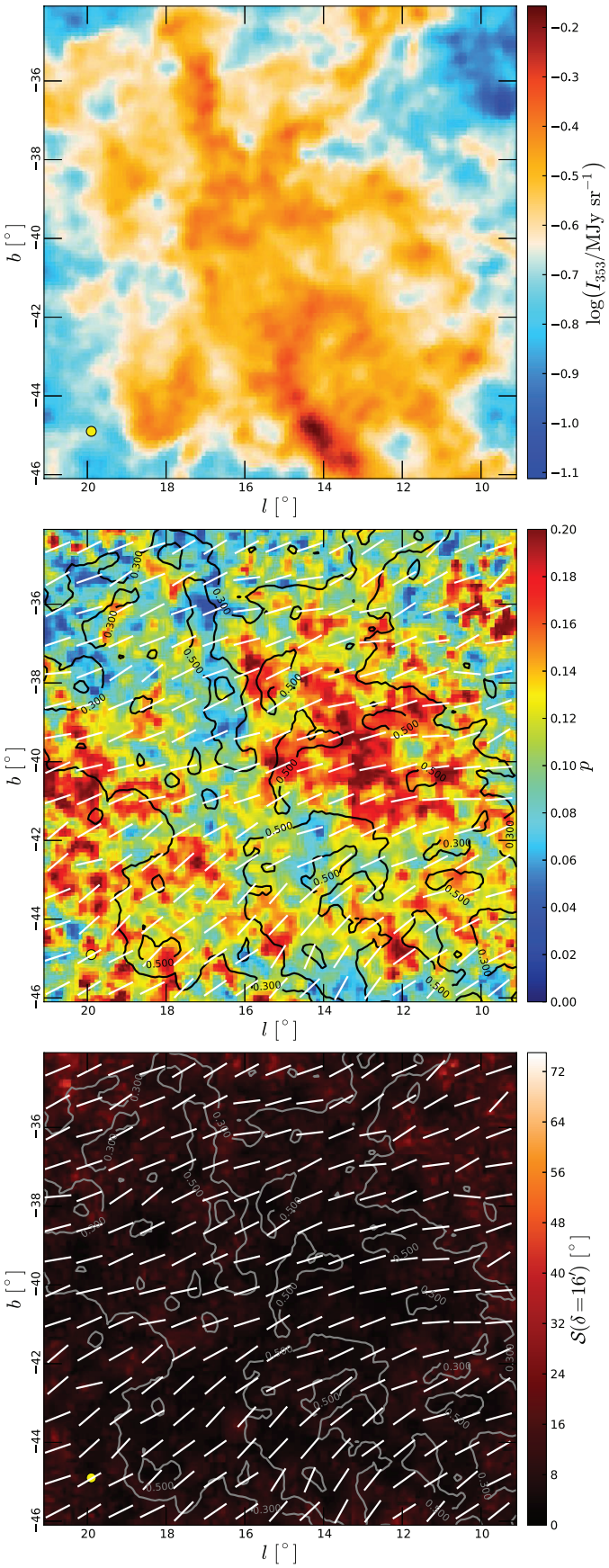

Fig. A.4. Same as Fig. 3, but for the Microscopium field.

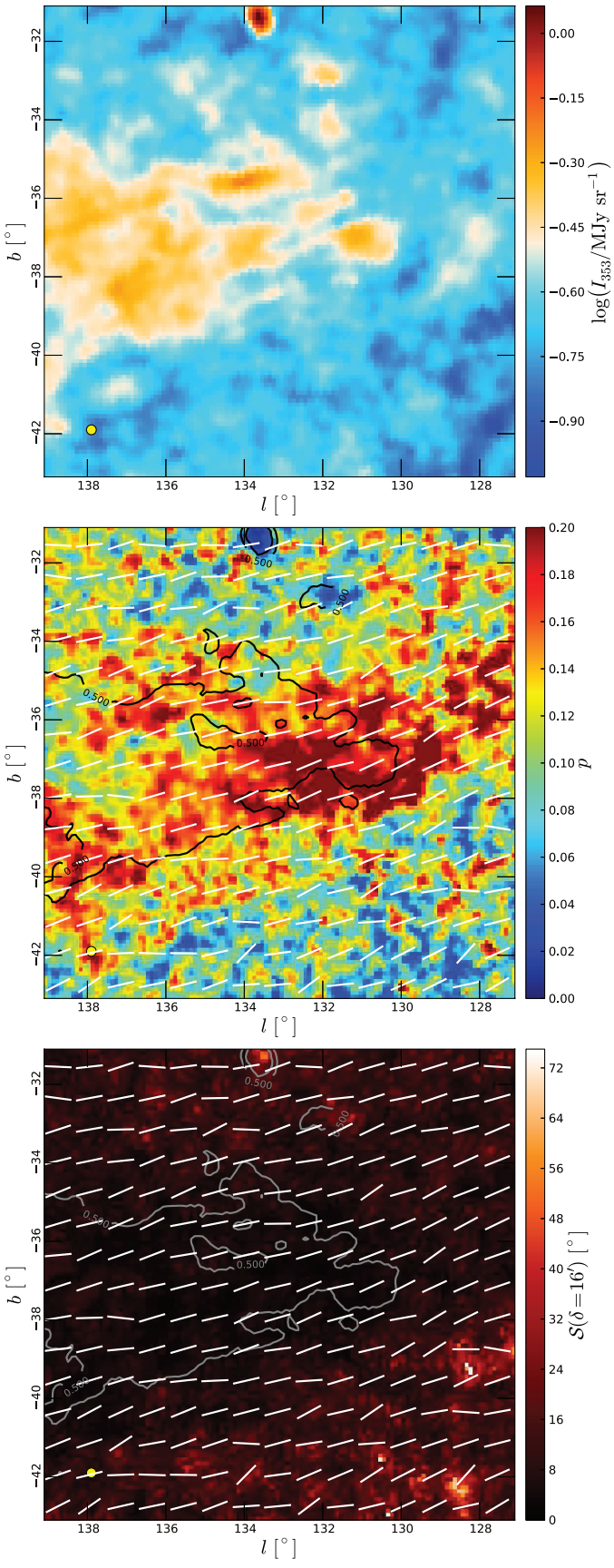

Fig. A.5. Same as Fig. 3, but for the Pisces field.

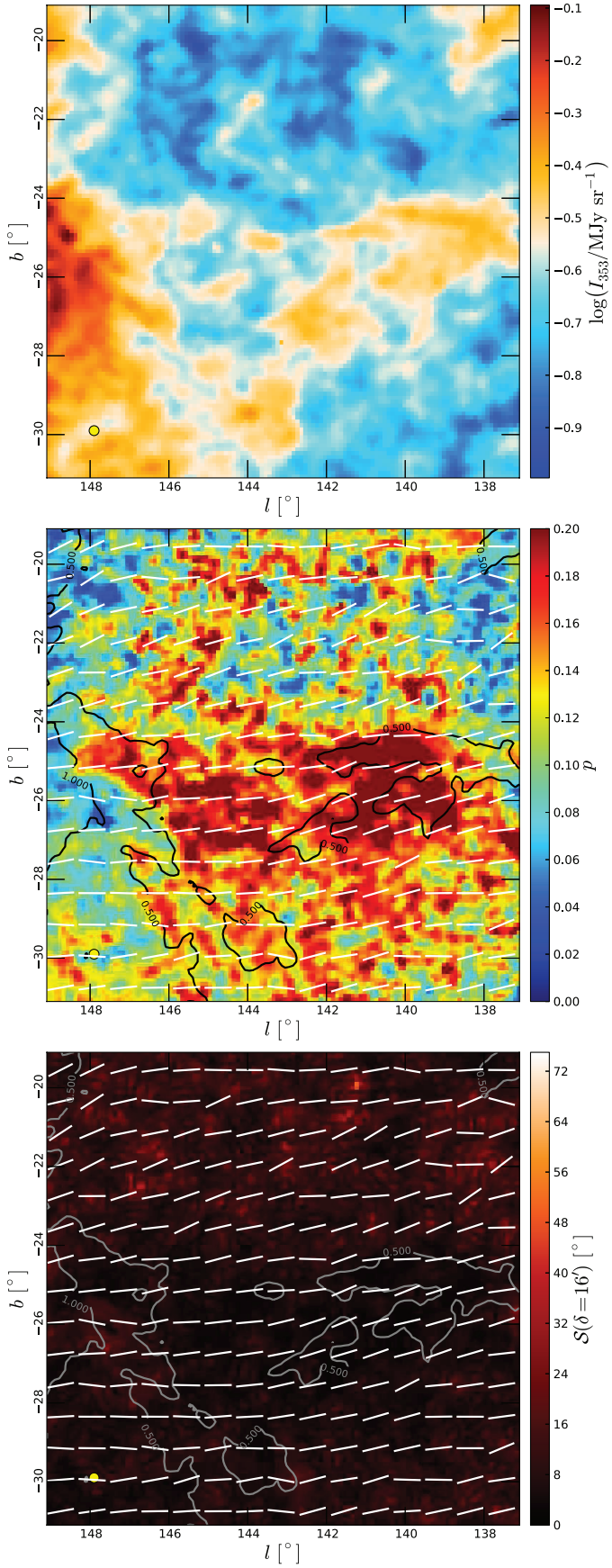

Fig. A.6. Same as Fig. 3, but for the Perseus field.

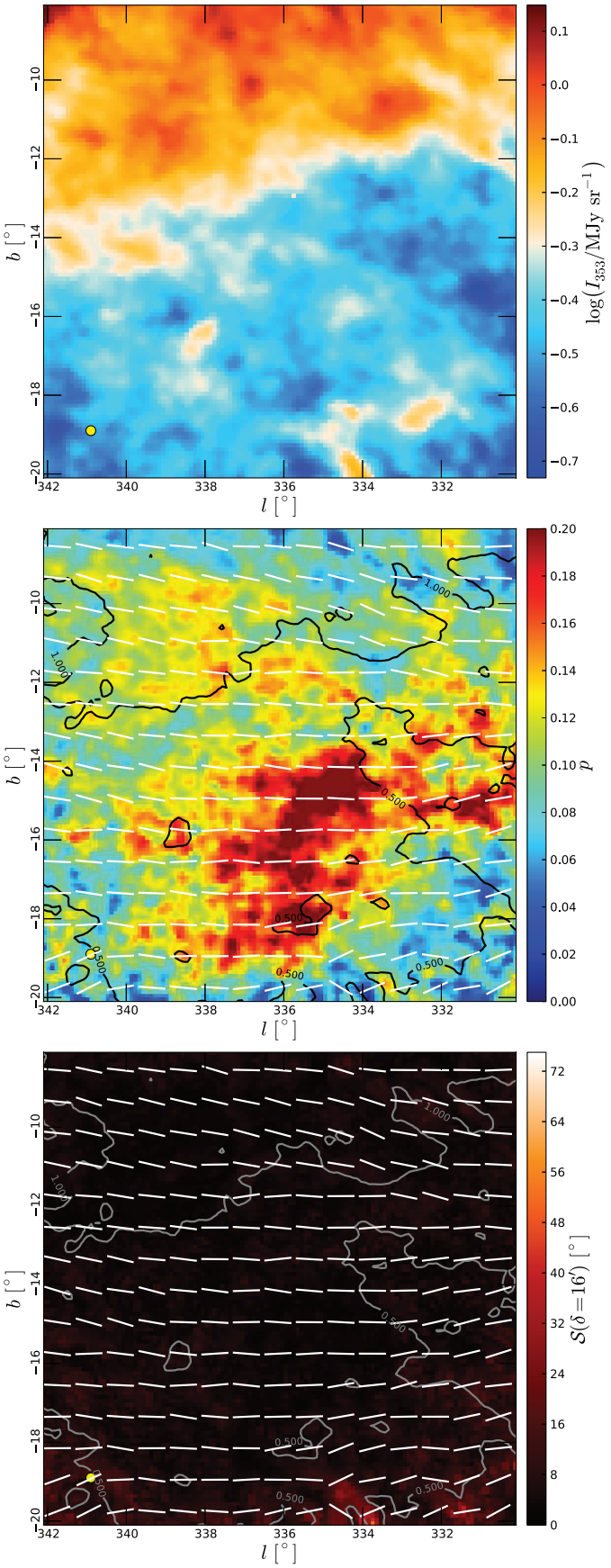

Fig. A.7. Same as Fig. 3, but for the Ara field.

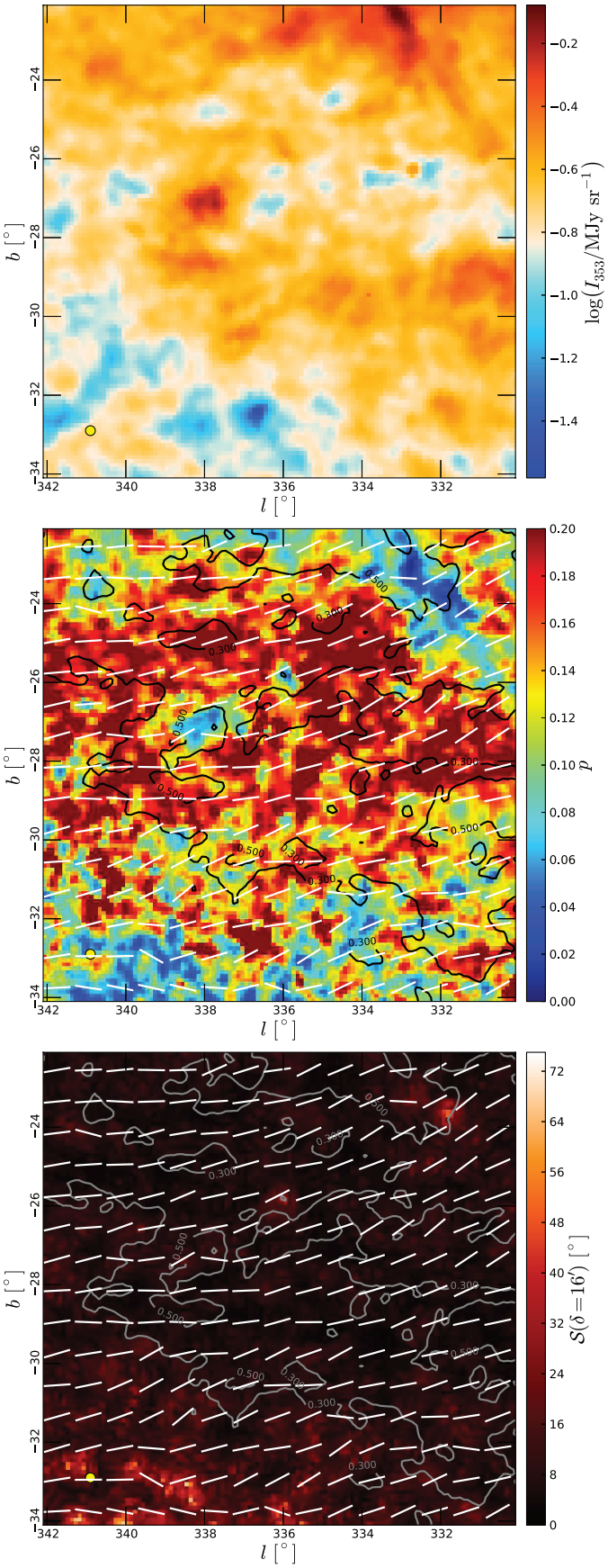

Fig. A.8. Same as Fig. 3, but for the Pavo field.

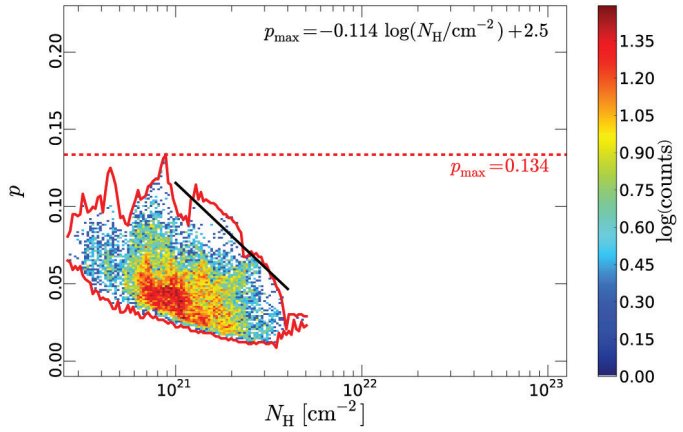

Fig. A.9. Same as Fig. 4, but for the Polaris Flare field. Two-dimensional distribution function of polarization fraction p and column density $N_{\rm H}$. The distribution function is presented in logarithmic colour scale and includes only points for which $p/\sigma_p > 3$. The dashed red line corresponds to the absolute maximum polarization fraction $p_{\rm max}$ and the solid red curves show the upper and lower envelopes of p as functions of $N_{\rm H}$. The solid black line is a linear fit $p_{\rm max} = m \log\left(N_{\rm H}/{\rm cm}^{-2}\right) + c$ to the decrease of the maximum polarization fraction with column density at the high end of $N_{\rm H}$ (see Table 2 for the fitting ranges and fit parameters).

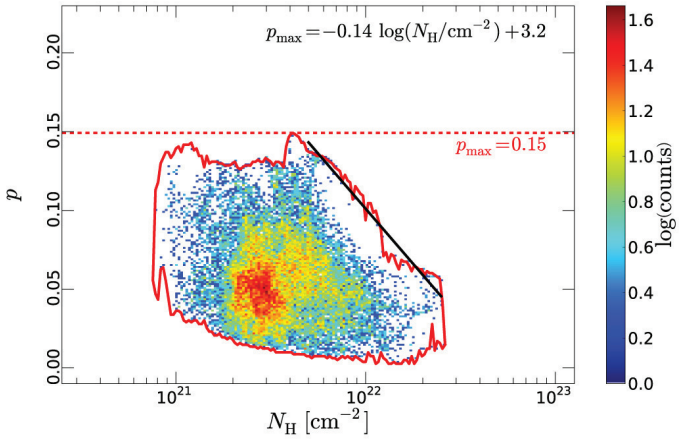

Fig. A.10. Same as Fig. 4, but for the Taurus field.

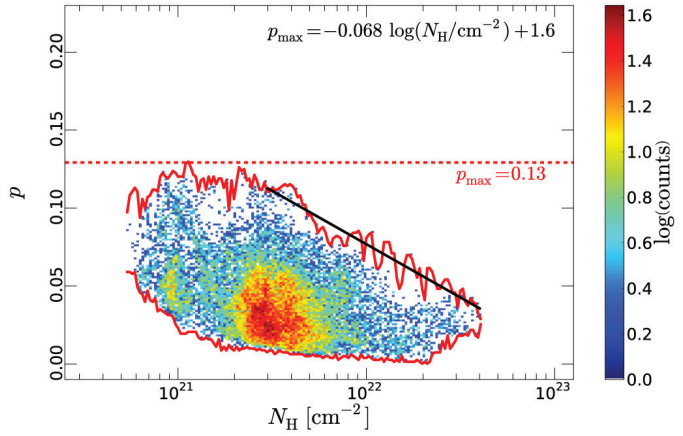

Fig. A.11. Same as Fig. 4, but for the Orion field.

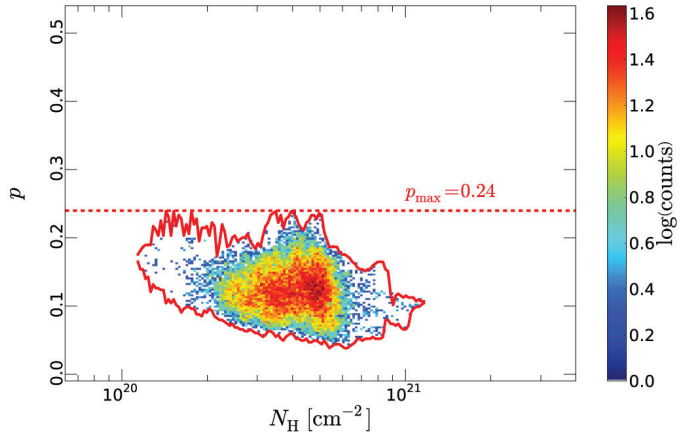

Fig. A.12. Same as Fig. 4, but for the Microscopium field. Note that the ranges in $N_{\rm H}$ and p are different from Fig. 4, and that no fit is performed.

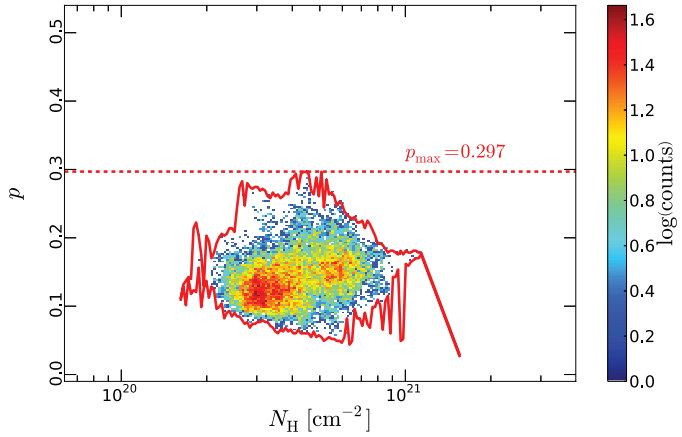

Fig. A.13. Same as Fig. 4, but for the Pisces field. Note that the ranges in $N_{\rm H}$ and p are different from Fig. 4, and that no fit is performed.

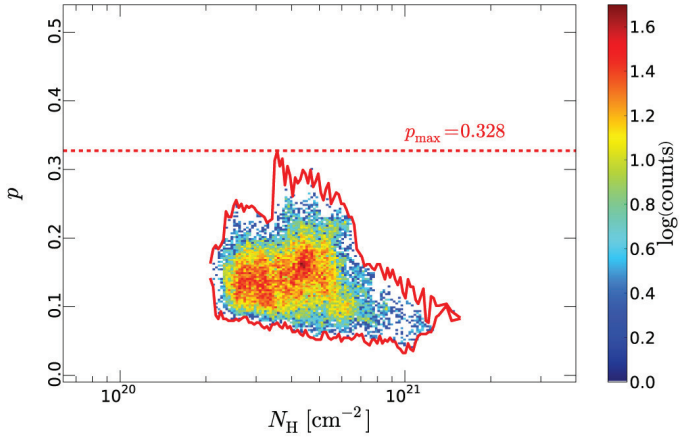

Fig. A.14. Same as Fig. 4, but for the Perseus field. Note that the ranges in $N_{\rm H}$ and p are different from Fig. 4, and that no fit is performed.

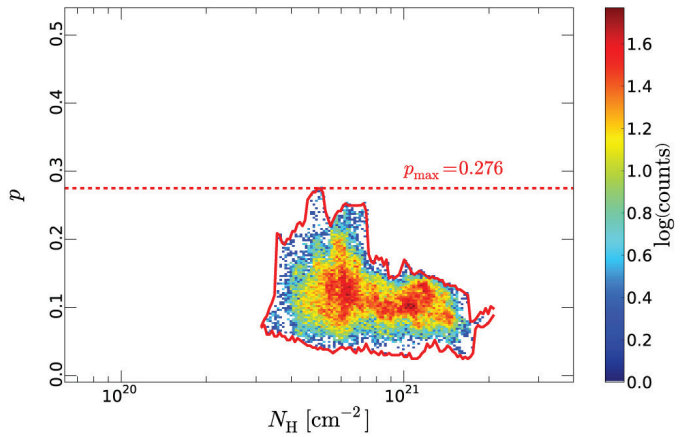

Fig. A.15. Same as Fig. 4, but for the Ara field. Note that the ranges in $N_{\rm H}$ and p are different from Fig. 4, and that no fit is performed.

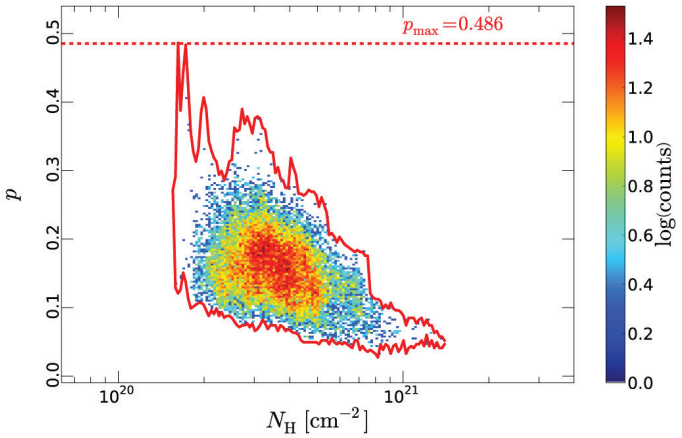

Fig. A.16. Same as Fig. 4, but for the Pavo field. Note that the ranges in $N_{\rm H}$ and p are different from Fig. 4, and that no fit is performed.

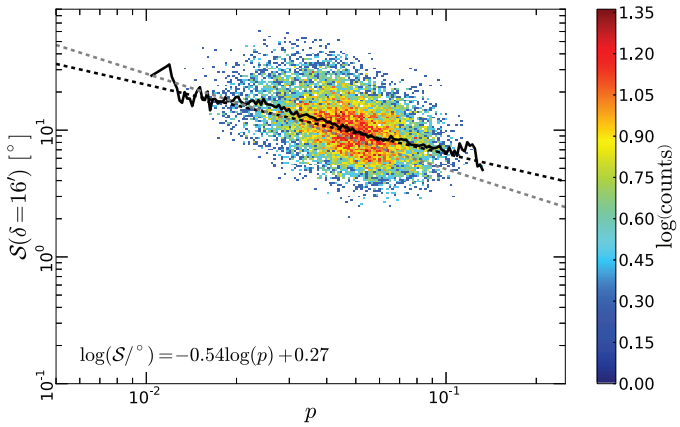

Fig. A.17. Same as Fig. 7, but for the Polaris Flare field. Two-dimensional distribution function of $\mathcal{S}$ and polarization fraction p. The angle dispersion function $\mathcal{S}$ is computed at a lag $\delta = 16'$. Only pixels for which $p/\sigma_p > 3$ are retained. The dashed grey line is the large-scale fit (with $FWHM = 1^\circ$ and $\delta = 1.^\circ07$) $\log(\mathcal{S}) = -0.75\log(p) - 0.06$, the solid black line shows the mean $\mathcal{S}$ for each bin in p (the bin size is $\Delta\log(p) = 0.008$) and the dashed black line is a linear fit of that curve in log-log space, restricted to bins in p which contain at least 1% of the total number of points (so about 150 points per bin).

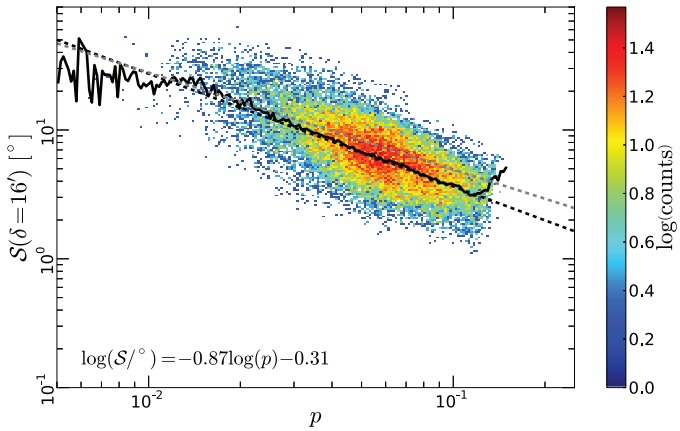

Fig. A.18. Same as Fig. 7, but for the Taurus field.

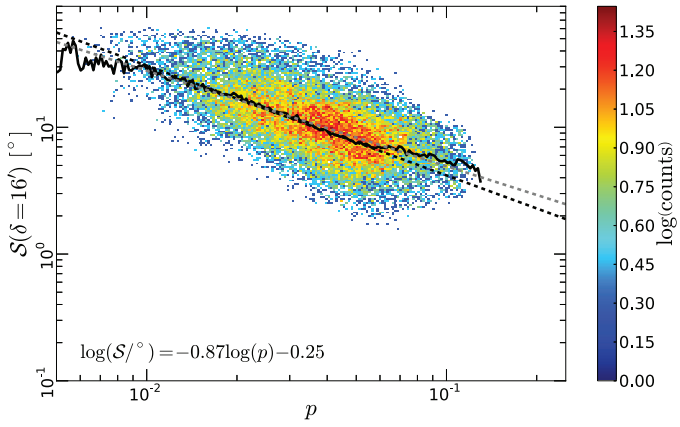

Fig. A.19. Same as Fig. 7, but for the Orion field.

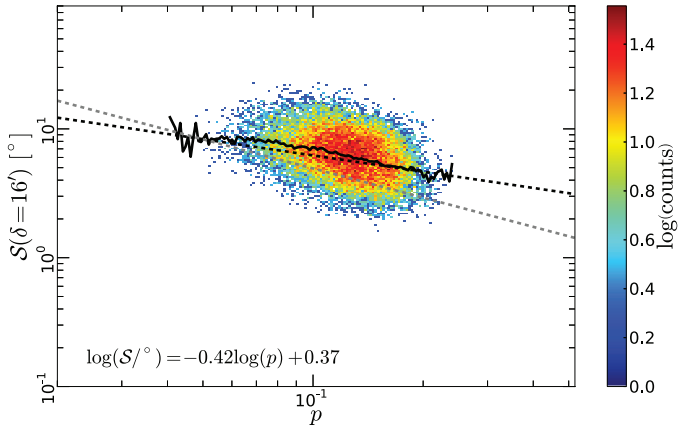

Fig. A.20. Same as Fig. 7, but for the Microscopium field. Note that the range in p is different from Fig. 7.

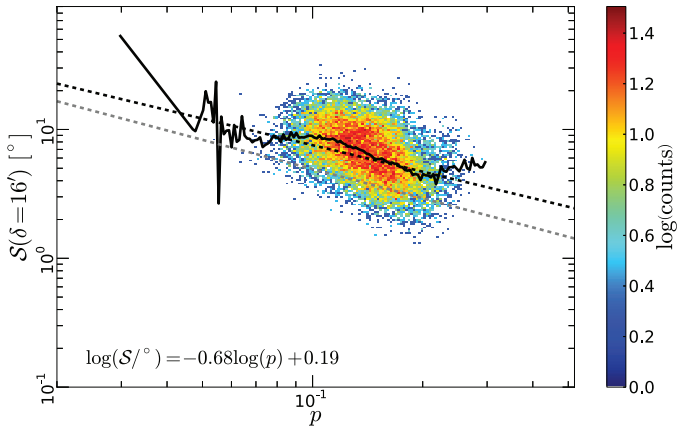

Fig. A.21. Same as Fig. 7, but for the Pisces field. Note that the range in p is different from Fig. 7.

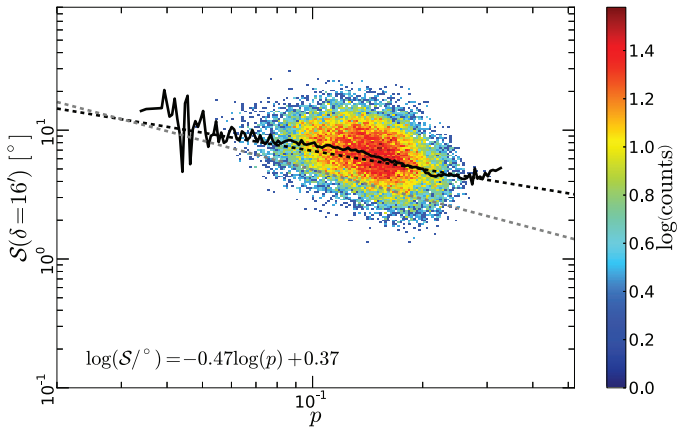

Fig. A.22. Same as Fig. 7, but for the Perseus field. Note that the range in p is different from Fig. 7.

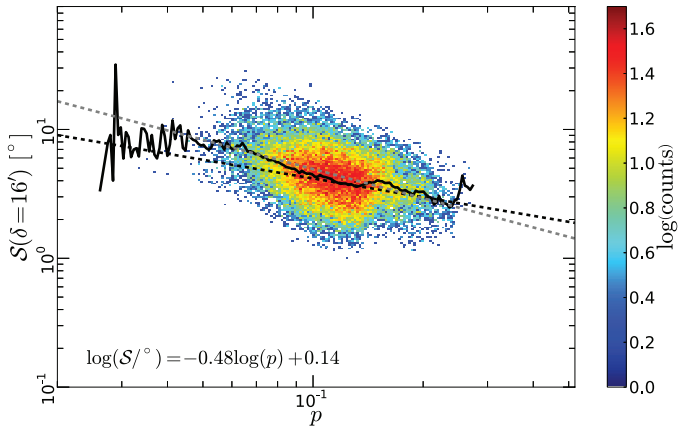

Fig. A.23. Same as Fig. 7, but for the Ara field. Note that the range in p is different from Fig. 7.

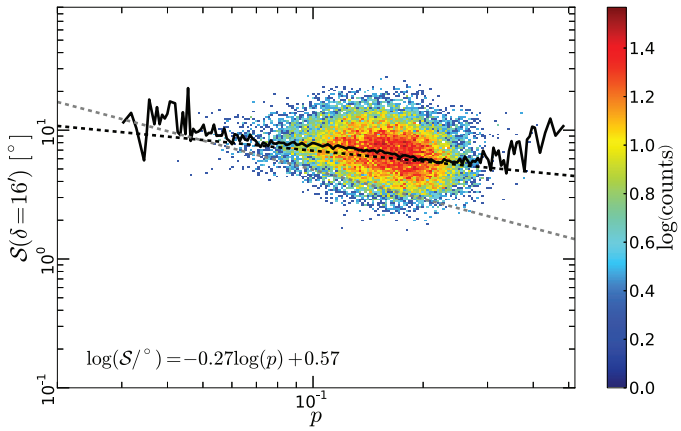

Fig. A.24. Same as Fig. 7, but for the Pavo field. Note that the range in p is different from Fig. 7.

Appendix B: Derivation of the Stokes parameters for emission

The derivation of the Stokes equations Eqs. (5)–(7), as presented by Wardle & Königl (1990) based upon Lee & Draine (1985), considers the extinction cross sections $C_\parallel$ and $C_\perp$ for light that is polarized parallel or perpendicular to the grain symmetry axis, and distinguishes oblate and prolate grains. Say that at each point M on the line of sight we define a reference frame $(Mx_0y_0z_0)$ such that z_0 points to the observer, and the local magnetic field $\boldsymbol{B}$ is in the (My_0z_0) plane. With β the angle between $\boldsymbol{B}$ and the angular momentum $\boldsymbol{J}$ of a rotating grain at M, and γ the angle between $\boldsymbol{B}$ and the plane of the sky, as defined in Fig. 14, Lee & Draine (1985) give, for oblate grains

$$C_{x_0} = C_\perp - \frac{C_\perp - C_\parallel}{2}\sin^2\beta \tag{B.1}$$

$$C_{y_0} = C_\perp - \frac{C_\perp - C_\parallel}{2}\left[\sin^2\beta + \cos^2\gamma\left(3\cos^2\beta - 1\right)\right] \tag{B.2}$$

and for prolate grains

$$C_{x_0} = C_\perp + \frac{C_\parallel - C_\perp}{4}\left(1 + \cos^2\beta\right) \tag{B.3}$$

$$C_{y_0} = C_\perp + \frac{C_\parallel - C_\perp}{4}\left[1 + \cos^2\beta - \cos^2\gamma\left(3\cos^2\beta - 1\right)\right]. \tag{B.4}$$

For spherical grains, all these cross-sections are of course equal, $C_{x_0} = C_{y_0} = C_\perp = C_\parallel$. The expressions for the Stokes parameters in terms of the cross-sections are

$$I = \int n_\mathrm{d} B_\nu(T_\mathrm{d})\,\frac{\langle C_{x_0} + C_{y_0}\rangle}{2}\mathrm{d}s \tag{B.5}$$

$$Q = \int n_\mathrm{d} B_\nu(T_\mathrm{d})\,\frac{\langle C_{x_0} - C_{y_0}\rangle}{2}\cos(2\phi)\,\mathrm{d}s \tag{B.6}$$

$$U = \int n_\mathrm{d} B_\nu(T_\mathrm{d})\,\frac{\langle C_{x_0} - C_{y_0}\rangle}{2}\sin(2\phi)\,\mathrm{d}s \tag{B.7}$$

where the average $\langle\ldots\rangle$ is performed on the possible angles β. The equivalent expressions given by Wardle & Königl (1990) are incorrect in omitting the factor 1/2 (it is easily checked that our expressions match the expected form of I in the case of spherical grains, and of P/I in the case of fully polarizing grains: 100% polarization when $C_{y_0} = 0$.

Computation of the sums and differences of C_{x_0} and C_{y_0} for both grain geometries leads to the same expressions for the Stokes parameters

$$I = \int n_\mathrm{d} B_\nu(T_\mathrm{d})\,C_\mathrm{avg}\left[1 - p_0\left(\cos^2\gamma - \frac{2}{3}\right)\right]\mathrm{d}s \tag{B.8}$$

$$Q = \int n_\mathrm{d} B_\nu(T_\mathrm{d})\,C_\mathrm{avg} p_0\cos(2\phi)\cos^2\gamma\,\mathrm{d}s \tag{B.9}$$

$$U = \int n_\mathrm{d} B_\nu(T_\mathrm{d})\,C_\mathrm{avg} p_0\sin(2\phi)\cos^2\gamma\,\mathrm{d}s \tag{B.10}$$

where we have introduced the average cross-section

$$C_\mathrm{avg} = \frac{1}{3}\left(2C_\perp + C_\parallel\right), \tag{B.11}$$

and the polarization cross section

$$C_\mathrm{pol} = \frac{C_\perp - C_\parallel}{2} \qquad \text{(for oblate grains)} \tag{B.12}$$

$$C_\mathrm{pol} = \frac{C_\parallel - C_\perp}{4} \qquad \text{(for prolate grains).} \tag{B.13}$$

These expressions match those in Martin (1972), Martin (1974), Martin (1975), and Draine & Fraisse (2009); those adopted by Lee & Draine (1985) are a factor 2 larger. The parameter p_0 is then given by

$$p_0 = \frac{C_\mathrm{pol}}{C_\mathrm{avg}}\frac{3}{2}\left(\langle\cos^2\beta\rangle - \frac{1}{3}\right) = \frac{C_\mathrm{pol}}{C_\mathrm{avg}}R \tag{B.14}$$

with R a Rayleigh reduction factor accounting for the chosen form of imperfect alignment (Lee & Draine 1985). Writing the equations for I, Q and U using the optical depth τ_ν (which is small in the submillimetre) in place of the physical position s on the line of sight, one is led to Eqs. (5)–(7).

The intrinsic polarization fraction is easily computed for both grain geometries:

$$p_\mathrm{i} = \frac{C_\perp - C_\parallel}{C_\perp + C_\parallel} \qquad \text{(for oblate grains)} \tag{B.15}$$

$$p_\mathrm{i} = \frac{C_\parallel - C_\perp}{3C_\perp + C_\parallel} \qquad \text{(for prolate grains).} \tag{B.16}$$